



LAWRENCE  
LIVERMORE  
NATIONAL  
LABORATORY

LLNL-TR-854972

# Bayesian inference for the seismic moment tensor using regional waveforms and a data-derived distribution of velocity models

A. Chiang, S. Ford, M. Pasmanos

September 27, 2023

## **Disclaimer**

---

This document was prepared as an account of work sponsored by an agency of the United States government. Neither the United States government nor Lawrence Livermore National Security, LLC, nor any of their employees makes any warranty, expressed or implied, or assumes any legal liability or responsibility for the accuracy, completeness, or usefulness of any information, apparatus, product, or process disclosed, or represents that its use would not infringe privately owned rights. Reference herein to any specific commercial product, process, or service by trade name, trademark, manufacturer, or otherwise does not necessarily constitute or imply its endorsement, recommendation, or favoring by the United States government or Lawrence Livermore National Security, LLC. The views and opinions of authors expressed herein do not necessarily state or reflect those of the United States government or Lawrence Livermore National Security, LLC, and shall not be used for advertising or product endorsement purposes.

This work performed under the auspices of the U.S. Department of Energy by Lawrence Livermore National Laboratory under Contract DE-AC52-07NA27344.

1 Bayesian inference for the seismic moment tensor using regional  
2 waveforms and a data-derived distribution of velocity models

3 Andrea Chiang\*, Sean Ford and Mike Pasyanos

Lawrence Livermore National Laboratory, Livermore, California 94550, USA

\*Corresponding author, chiang4@llnl.gov

4 September 27, 2023

5 **Abstract**

6 The largest source of uncertainty in any source inversion is the velocity model used to construct the  
7 transfer function employed in the forward model that relates observed ground motion to the seismic  
8 moment tensor. However, standard inverse procedures often does not quantify uncertainty in the seismic  
9 moment tensor due to error in the Green's functions from uncertain event location and Earth structure.  
10 We attempt to incorporate this uncertainty into an estimation of the seismic moment tensor using a  
11 distribution of velocity models calculated in a prior effort based on different and complementary data  
12 sets. The posterior distribution of velocity models is then used to construct Green's functions for use in  
13 Bayesian inference of an unknown seismic moment tensor using regional waveform data. The combined  
14 likelihood is estimated using data-specific error models and the posterior of the seismic moment tensor  
15 is estimated and can be interpreted in terms of most-probable source-type.

16 **1 Introduction**

17 The seismic moment tensor (MT) has long been used in earthquake and explosion source analysis, and there  
18 has been a renewed interest in how it can inform us about the seismic source particularly in the geophysical  
19 monitoring community due to its application in event identification and yield analysis (Ford et al., 2020;  
20 Pasyanos & Chiang, 2022). Some of this interest derives from our recent ability to routinely determine  
21 six-component MT that takes advantage of the full description of the MT to characterize isotropic and  
22 non-isotropic radiation of seismic sources. The elements of the tensor are used to derive the source-type  
23 and subsequently tested against theoretical mechanisms such as explosion, earthquake and collapse. MTs  
24 and their source-types have been shown to be valuable geophysical monitoring tools in identifying explosions  
25 (Alvizuri et al., 2018; Chiang et al., 2018; Mustać et al., 2020) and other nuisance signals, as well as  
26 discriminating explosions from earthquakes when varied-data type inversion is applied to the analysis. The  
27 MTs can be used to augment traditional semi-empirical based methods that utilize surface-to-body-wave  
28 magnitude ratios (Selby et al., 2012) and regional phase amplitude ratios (Bottone et al., 2002; Walter et al.,  
29 2018). The effort to develop and improve the MT discriminant for monitoring and enforcement of nuclear  
30 test-ban treaties continue to be an area of active research.

31 However, parameter uncertainties in seismic MT inversion are rarely available. The inverse procedure  
32 often does not quantify MT model errors such as event location, data noise and Earth model that are

33 essential for estimating solution robustness. Here we propose to adopt the Bayesian probabilistic framework  
 34 to incorporate uncertainties in MT inversions. The probabilistic formulation described by Tarantola and  
 35 Valette (1982) casts the inverse problem in a Bayesian framework where information on the model parameters  
 36 is represented in probabilistic term. With this approach the solution is given as the complete posterior  
 37 probability density function of the data and model parameters, instead of a single best-fit solution.

## 38 2 Method

39 The seismic MT is a  $3 \times 3$  matrix consists of nine force couples that represent the equivalent body forces  
 40 for seismic sources of different geometries, which due to conservation of angular momentum reduce to six  
 41 independent couples and dipoles. In the Bayesian framework, an appropriate choice of a priori moment tensor  
 42 probability is important, but what constitutes as a random moment tensor is not straightforward and depends  
 43 on the coordinate domain of the parameterized MT. Tape and Tape (2015) have shown that uniformly  
 44 distributed MTs have uniformly distributed orientations (eigenvectors) but not uniformly distributed source-  
 45 types (eigenvalues). In fact uniformly distributed MTs favors double-couples in the source-type space.

46 Tape and Tape (2015) have provided two approaches to generate uniformly distributed moment tensors  
 47 based on the 5-D space of all MTs of unit norm, in which one of the approaches uses a parameterization of  
 48 the MT that is closely related to the MT orientations and source types. The Tape parameterization has five  
 49 parameters and have finite upper and lower bounds:  $\kappa$  (strike),  $h$  (dip cosine),  $\sigma$  (slip),  $u$  (similar to lune  
 50 colatitude) and  $v$  (similar to lune longitude), where the pair  $(u, v)$  determines the normalized eigenvalues of  
 51 MT (source type). We can now construct the uniform priors using the five Tape parameterization and the  
 52 seismic moment.

53 Observed data is related to the seismic MT via a transfer function that is the Green's function for  
 54 the path from source to receiver. We employ the principle of reciprocity (e.g. Dahlen & Tromp, 1998) to  
 55 produce Green's functions for many source locations and one station location. Zhao et al. (2006) shows  
 56 that the component  $n$  of displacement  $u_n$  at receiver location  $\mathbf{x}$  from source location  $\mathbf{x}'$  is related to the  
 57 spatial gradient of the Green's tensor  $\partial_i G_{nj}(\mathbf{x}, \mathbf{x}'; t)$  where  $i, j = 1, 2, 3$  are the cartesian spatial components.  
 58 Betti's theorem (i.e., reciprocity) states that the spatial gradient of the Green's tensor from source to receiver  
 59 is equal to the strain Green's tensor from receiver to source  $(\partial_i G_{jn}(\mathbf{x}', \mathbf{x}; t) + \partial_j G_{in}(\mathbf{x}', \mathbf{x}; t))/2$ , which is  
 60 composed of spatial gradients of the Green's tensor from receiver to source.

61 We use reciprocity as described by Eisner and Clayton (2001) to calculate the displacement gradients  
 62 in SW4 (Petersson & Sjögren, 2017) for a grid of event epicenters, depths, and origin times centered on  
 63 the USGS solution. The epicentral and depth range are  $\pm 3$  km and 600 to 2400 m in 600 m steps, and the  
 64 time range is  $\pm 0.2$  s in 0.1 s steps, which results in 2420 origins. The Green's functions for these origins  
 65 are calculated over many velocity model realizations from the posterior calculated in Pasyanos et al. (2006).  
 66 Figure 1 is a reproduction from that work showing the mean upper mantle velocity and corresponding  
 67 uncertainty.

68 Graves and Wald (2001) lays out the forward model for component  $n$  of displacement  $u$  at the receiver

$$u_n = a_1 \times mxx_n + a_2 \times myy_n + a_3 \times mzz_n + a_4 \times mxy_n + a_5 \times mxz_n + a_6 \times myz_n. \quad (1)$$

69 The coefficients  $(a_1, \dots, a_6)$  are the moment tensor elements and the predictor variables  $(mxx_n, \dots, myz_n)$  are  
 70 components of the strain Green's tensor for a single force in direction  $n$  imposed at the receiver recorded at

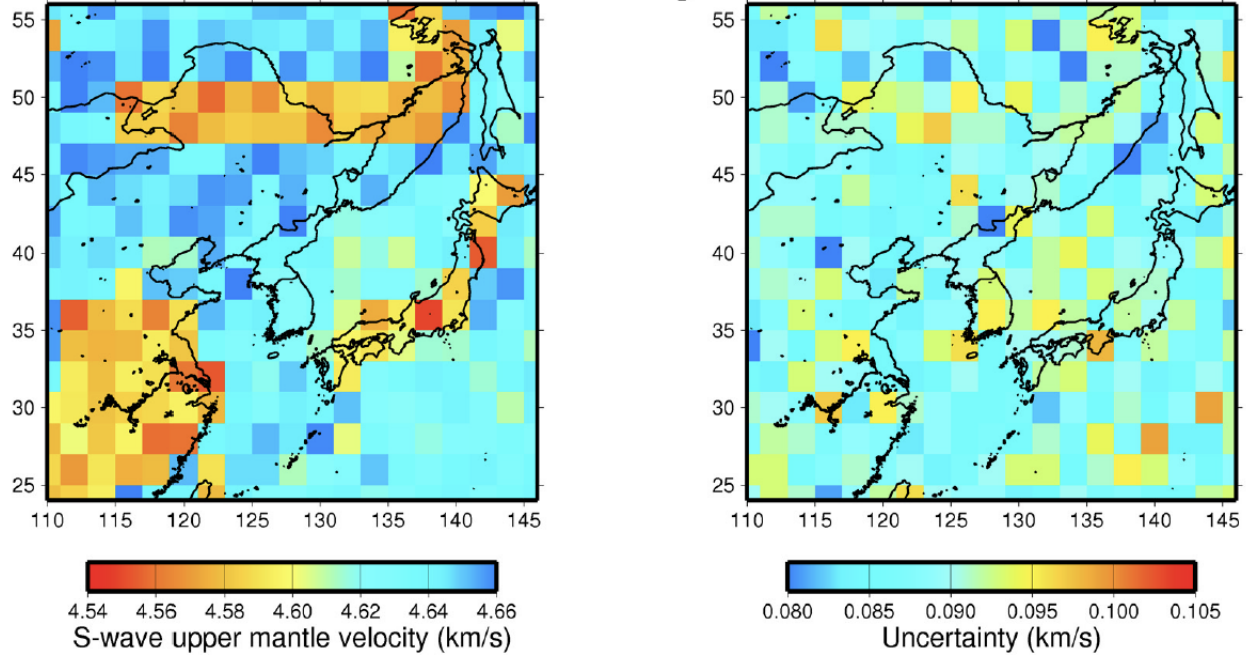


Figure 1: Figure 13 from Pasyanos et al., 2006. Map of upper mantle S wave velocities and corresponding uncertainties for the YSKP region.

71 the source. For each of the 3 components  $n = x, y, z$  we have 6 elements of the strain Green's tensor,

$$\begin{aligned}
 mxx &= \partial u_x / \partial x \\
 myy &= \partial u_y / \partial y \\
 mzz &= \partial u_z / \partial z \\
 mxy &= \partial u_y / \partial x + \partial u_x / \partial y \\
 mxz &= \partial u_z / \partial x + \partial u_x / \partial z \\
 myz &= \partial u_z / \partial y + \partial u_y / \partial z
 \end{aligned} \tag{2}$$

72 In order to output the  $mij$  waveforms for each source location in SW4 we make three calculations; one for  
 73 each direction of a single force applied at the receiver location and recorded at the source locations using the  
 74 **strains** output. The off-diagonal  $mij$  waveforms are multiplied by two to account for the moment tensor  
 75 source symmetry.

76 The data covariance is modeled after the observations. This is a preferred approach because now the  
 77 residuals are “weighted” by a realistic covariance and not an a priori weighting scheme (e.g., Chen et al.,  
 78 2015). Figure 2 shows the zero-lag covariance used in the method.

79 We use 5 million sources to uniformly cover the source space and transform them to moment tensor  
 80 elements.

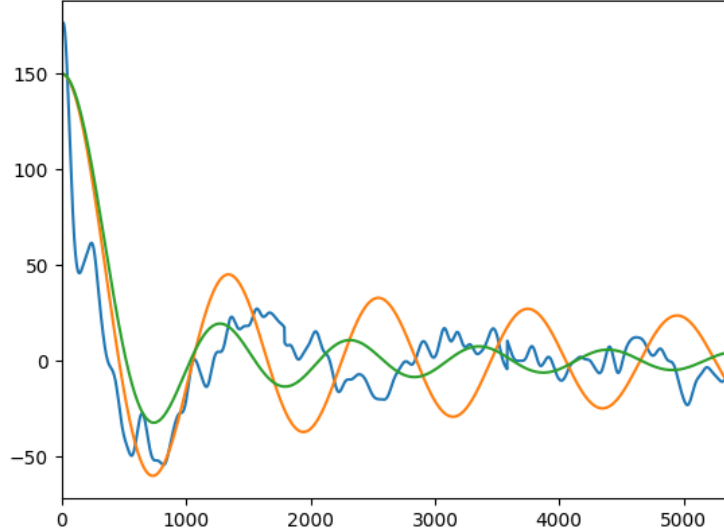


Figure 2: Empirical (blue) and analytical covariance functions. The analytical functions are bessel (orange) and sinc (green).

### 81 3 Case Study: DPRK09

82 In 2009, the Democratic Peoples Republic of Korea (DPRK) announced a nuclear test at the Punggyi-Ri  
 83 Test Site. Kim and Richards (2007) and Koper et al. (2008) show initial discrimination and the USGS  
 84 location of the event.

85 We will employ the intermediate displacement waveforms from stations MDJ and INCN for the moment  
 86 tensor inference. Figure 3 shows the observation at MDJ and INCN in orange along with predictions using  
 87 an MT for the explosion from Chiang et al. (2018) for several velocity models and source locations.

88 Here we represent the MT inversion result in terms of the marginal likelihood on the lune. Figure 4  
 89 shows the marginal likelihood for a single station inversion (MDJ) and the combined marginal likelihood  
 90 from stations MDJ and INCN. The best solutions are predominantly isotropic as indicated by the darker  
 91 colors near the poles. For the single station inversion, the most probable MT solutions are distributed between  
 92 the positive and negative isotropic, but incorporating waveform data from INCN significantly improves the  
 93 uncertainties in the MT solutions by eliminating the implosive sources. The combined marginal likelihood  
 94 shows the most probable solutions are explosive in nature consistent with an underground explosion event.

### 95 4 Future work

96 Future work will be to produce more likelihood surfaces for the regional waveform data type and incorporate  
 97 the additional data type of teleseismic-P. We will also sample the posterior using an MCMC approach and  
 98 compare with the grid-based posterior calculation approach described here.

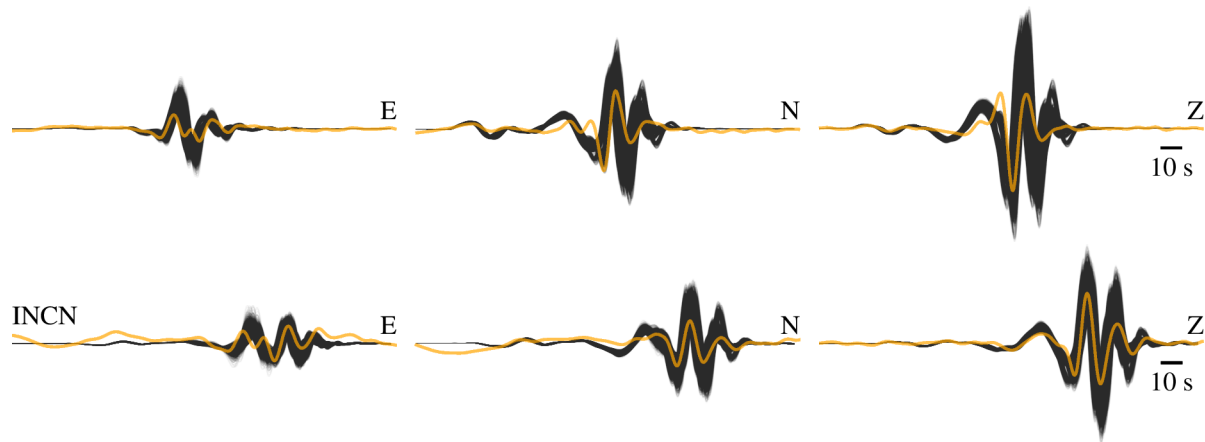


Figure 3: Observation of DPRK09 at MDJ (top) and INCN (orange) compared with predictions for a DPRK09 MT (Chiang et al., 2018) using 8 velocity models, 484 locations, and 5 origin times.

## 99 References

100 Alvizuri, C., Silwal, V., Krischer, L., & Tape, C. (2018). Estimation of Full Moment Tensors, Including  
 101 Uncertainties, for Nuclear Explosions, Volcanic Events, and Earthquakes. *Journal of Geophysical*  
 102 *Research*, 123(6). <https://doi.org/10.1029/2017JB015325>

103 Bottone, S., Fisk, M. D., & McCartor, G. D. (2002). Regional Seismic-Event Characterization Using a  
 104 Bayesian Formulation of Simple Kriging. *Bulletin of the Seismological Society of America*, 92(6),  
 105 2277–2296. <https://doi.org/10.1785/0120010141>

106 Chen, W., Ni, S., Kanamori, H., Wei, S., Jia, Z., & Zhu, L. (2015). CAPjoint, A Computer Software Package  
 107 for Joint Inversion of Moderate Earthquake Source Parameters with Local and Teleseismic Wave-  
 108 forms. *Seismological Research Letters*, 86, 432–441. <https://doi.org/10.1785/0220140167>

109 Chiang, A., Ichinose, G. A., Dreger, D. S., Ford, S. R., Matzel, E. M., Myers, S. C., & Walter, W. R. (2018).  
 110 Moment Tensor Source-Type Analysis for the Democratic People's Republic of Korea–Declared Nu-  
 111 clear Explosions (2006–2017) and 3 September 2017 Collapse Event. *Seismological Research Letters*.  
 112 <https://doi.org/10.1785/0220180130>

113 Dahlen, F. A., & Tromp, J. (1998). *Theoretical global seismology*. Princeton University Press.

114 Eisner, L., & Clayton, R. W. (2001). A Reciprocity Method for Multiple-Source Simulations. *Bulletin of the*  
 115 *Seismological Society of America*, 91(3), 553–560. <https://doi.org/10.1785/0120000222>

116 Ford, S. R., Kraft, G. D., & Ichinose, G. A. (2020). Seismic moment tensor event screening. *Geophysical*  
 117 *Journal International*, 221(1), 77–88. <https://doi.org/10.1093/gji/ggz578>

118 Graves, R. W., & Wald, D. J. (2001). Resolution analysis of finite fault source inversion using one- and three-  
 119 dimensional Green's functions: 1. Strong motions. *Journal of Geophysical Research: Solid Earth*,  
 120 106(B5), 8745–8766. <https://doi.org/10.1029/2000JB900436>

121 Kim, W.-Y., & Richards, P. G. (2007). North Korean nuclear test: Seismic discrimination low yield. *Eos*,  
 122 *Transactions American Geophysical Union*, 88(14), 158–161. <https://doi.org/10.1029/2007EO140002>

123 Koper, K. D., Herrmann, R. B., & Benz, H. M. (2008). Overview of Open Seismic Data from the North  
 124 Korean Event of 9 October 2006. *Seismological Research Letters*, 79(2), 178–185. <https://doi.org/10.1785/gssrl.79.2.178>

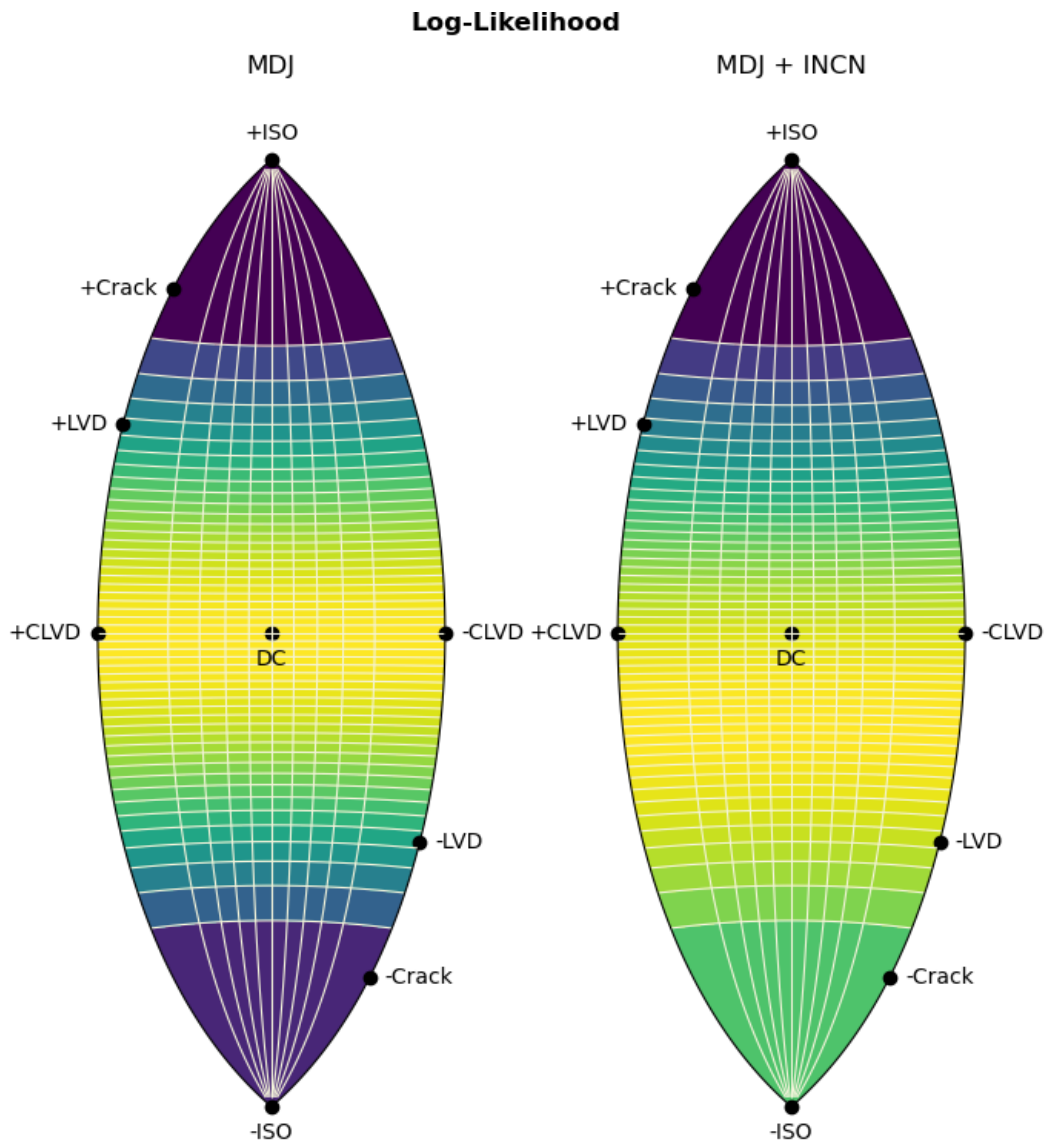


Figure 4: Marginal likelihoods for one velocity model.

126 Mustać, M., Hejrani, B., Tkalcic, H., Kim, S., Lee, S.-J., & Cho, C.-S. (2020). Large Isotropic Component in  
127 the Source Mechanism of the 2013 Democratic People's Republic of Korea Nuclear Test Revealed via  
128 a Hierarchical Bayesian Inversion. *Bulletin of the Seismological Society of America*, 110(1), 166–177.  
129 <https://doi.org/10.1785/0120190062>

130 Pasanos, M. E., & Chiang, A. (2022). Full Moment Tensor Solutions of U.S. Underground Nuclear Tests  
131 for Event Screening and Yield Estimation. *Bulletin of the Seismological Society of America*, 112(1),  
132 538–552. <https://doi.org/10.1785/0120210167>

133 Pasanos, M. E., Franz, G. A., & Ramirez, A. L. (2006). Reconciling a geophysical model to data using a  
134 Markov chain Monte Carlo algorithm: An application to the Yellow Sea–Korean Peninsula region.  
135 *Journal of Geophysical Research*, 111(B3). <https://doi.org/10.1029/2005jb003851>

136 Petersson, N. A., & Sjögren, B. (2017). *User's Guide to SW4, version 2.0*. Software Manual. Livermore,  
137 California, Lawrence Livermore National Laboratory. <https://doi.org/10.5281/zenodo.1045297>

138 Selby, N. D., Marshall, P. D., & Bowers, D. (2012). Mb:Ms Event Screening Revisited. *Bulletin of the  
139 Seismological Society of America*, 102(1). <https://doi.org/10.1785/0120100349>

140 Tape, W., & Tape, C. (2015). A uniform parametrization of moment tensors. *Geophysical Journal Interna-  
141 tional*, 202(3). <https://doi.org/10.1093/gji/ggv262>

142 Tarantola, A., & Valette, B. (1982). Inverse problems = quest for information. *Journal of Geophysics*, 50.

143 Walter, W. R., Dodge, D. A., Ichinose, G., Myers, S. C., Pasanos, M. E., & Ford, S. R. (2018). Body-Wave  
144 Methods of Distinguishing between Explosions, Collapses, and Earthquakes: Application to Recent  
145 Events in North Korea. *Seismological Research Letters*, 89(6), 2131–2138. <https://doi.org/10.1785/0220180128>

146 Zhao, L., Chen, P., & Jordan, T. H. (2006). Strain Green's Tensors, Reciprocity, and Their Applications  
147 to Seismic Source and Structure Studies. *Bulletin of the Seismological Society of America*, 96(5),  
148 1753–1763. <https://doi.org/10.1785/0120050253>